Integrated Thermal Silica Micro-Resonator Waveguide System With Ultra-Low Fluorescence

Christoph Pyrlik, Jan Schlegel, Florian Böhm, Andreas Thies, Olaf Krüger, Oliver Benson, Andreas Wicht, and Günther Tränkle

***Abstract*— Thermally grown silica is one of the most desirable materials for the realization of optical waveguides and whispering-gallery mode micro-resonators due to the ultra-low propagation loss and broad transparency window from UV to mid-IR. Here, we present the design, fabrication, and characterization of a high-Q ring-resonator device with a monolithically integrated evanescent rib waveguide coupler made solely from silica thermally grown on a Si substrate. The device delivered an intrinsic Q-factor of 3.7×10^6 and operated close to the critical coupling regime for both TE and TM polarizations. The achieved Q-factors were more than three orders of magnitude higher than those of comparable silica resonator devices. Furthermore, we showcase the ultra-low parasitic fluorescence unique to thermally grown silica and compare it to a device fabricated in Si_3N_4.**

***Index Terms*— Integrated optics, optical resonators, whispering-gallery modes.**

I. Introduction

HIGH-Q whispering-gallery mode (WGM) optical micro-resonators have gained considerable attention in the last decade. They combine high Q-factor, high energy density, and small footprint within a single device and hence allow for the miniaturization of optical setups in various fields of application, e.g. for the reduction of diode laser frequency noise with resonant optical feedback [1], as well as the realization of high efficient non-linear optics such as second harmonic generation [2]. Completely new applications such as the realization of Kerr combs have been demonstrated [3]. WGM micro-resonators have been fabricated in various geometries and with various fabrication technologies, e.g. micro-machining of crystals [4], or the realization of micro-disks with semiconductor technology [5].

Excitation of a WGM is achieved with an evanescent coupling device. Tapered optical fibers or prism couplers can be used, however, they require relatively bulky actuators to set the coupling gap, rendering the compactness of optical micro-resonators pointless. Semiconductor process technology, on the other hand, allows for the monolithic integration of an evanescent waveguide coupler as part of the same WGM resonator device. This eliminates the need for mechanical actuators that position the coupling device with respect to the WGM resonator. Monolithic integration provides scalability, reproducibility, and cost efficient fabrication common to semiconductor devices to the manufacturing of WGM resonators. Furthermore, this approach increases mechanical stability, ease of use, and allows for the development of more complex photonic integrated circuits consisting of multiple optical components on a chip. Recently, the potential of on-chip integrated WGM resonator devices has been demonstrated with the realization of a compact, ultra-fast optical ranging system suitable for LIDAR applications, that is based on two Kerr-combs generated in Si_3N_4 resonator chips [6].

Integrated WGM resonators fabricated with semiconductor process technology have already been realized in several different material systems. Si has been widely used in telecommunication applications, as demonstrated by Naiman et al. with Q-factors of 5.3×10^6 [7]. Other examples include Si_3N_4-based devices with intrinsic Q-factors reaching 170×10^6 [8], and diamond with 1×10^6 [9].

The apparent choice for many applications is silica thermally grown on silicon due to its broad transparency window covering UV to mid-IR, with corresponding ultra-low loss, and ultra-low parasitic fluorescence. Tapered fiber-coupled thermally grown silica resonators achieved record Q-factors of 875×10^6 [10]. However, the realization of wave-guiding and resonator structures in thermally grown silica necessitates the removal of Si beneath the waveguides to prevent the guided wave from leaking into the Si substrate.

An approach that circumvents the removal of Si is the use of dopants to create an index of refraction profile suitable for wave-guiding, Ferrera *et al.* [11] demonstrated Q-factors of 0.065×10^6 with this approach. Recently, Lee *et al.* [12] successfully demonstrated another approach that utilizes a Si_3N_4 waveguide that is processed in an additional step to access a silica micro-disk resonator, which delivered a Q-factor of 280×10^6. Both approaches introduce additional materials, which results in detrimental effects such as increased loss, fluorescence, and a smaller transparency window, which may render specific applications impossible.

Manuscript received October 17, 2018; revised January 20, 2019; accepted February 12, 2019. Date of publication February 18, 2019; date of current version March 12, 2019. This work was supported by the European Fund for Regional Development of the European Union in the Framework of Project iMiLQ, administrated by the Investitionsbank Berlin within the Program to Promote Research, Innovation, and Technologies (ProFIT) under Grant 10159465. *(Corresponding author: Christoph Pyrlik.)*

C. Pyrlik, J. Schlegel, A. Thies, O. Krüger, A. Wicht, and G. Tränkle are with the Ferdinand-Braun-Institut, Leibniz-Institut für Höchstfrequenztechnik, 12489 Berlin, Germany (e-mail: christoph.pyrlik@fbh-berlin.de).

F. Böhm and O. Benson are with the Institut für Physik, Humboldt-Universität zu Berlin, 12489 Berlin, Germany.

Color versions of one or more of the figures in this letter are available online at http://ieeexplore.ieee.org.

Digital Object Identifier 10.1109/LPT.2019.2899943

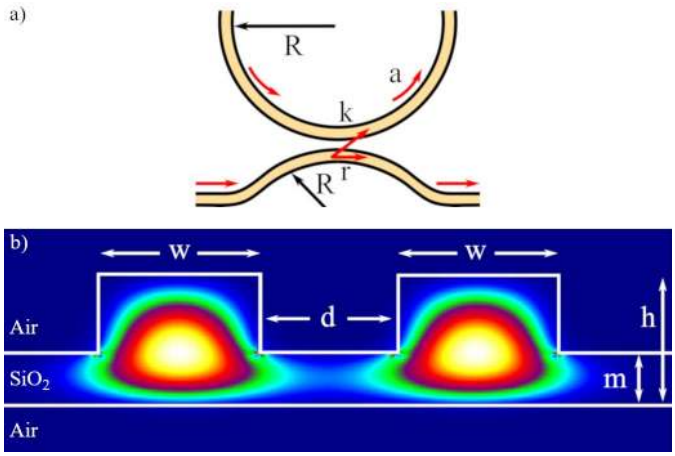

Fig. 1. a) Schematic of the symmetric coupler geometry with identical coupler and ring resonator radius R. The self-coupling, cross-coupling and single-pass transmission coefficients r, k, and a indicate the coupling directionality and round trip loss. b) shows the geometric cross-section of the ring-resonator and coupling waveguide. Their geometry parameters waveguide width w, oxide thickness h, and membrane thickness m are identical. They are separated by the coupling gap d. A false-color representation of the mode profiles for both fundamental modes is shown.

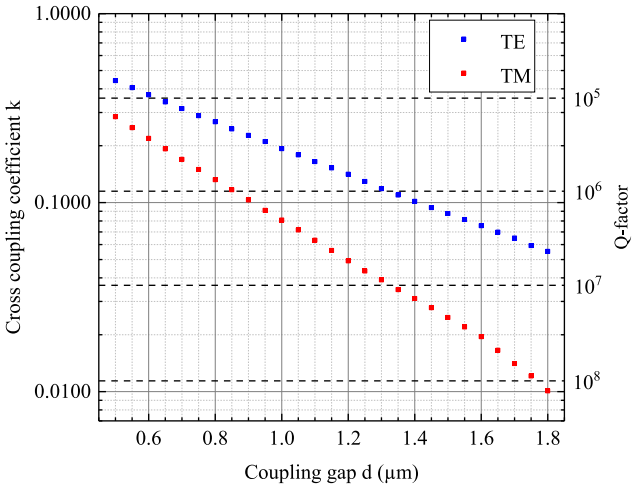

Fig. 2. The graph shows the numerically determined dependence of resonator Q-factor and amplitude coupling coefficient k on the coupling gap d under the assumption of critical coupling for both TE (blue) and TM (red) fundamental modes. Calculations were carried out for a ring-resonator and matching coupler radius $R = 0.5$ mm, and a rib geometry defined by $h = 2$ μm, $w = 1.4$ μm, and $m = 0.8$ μm.

Chen *et al.* [13] demonstrated a resonator system fabricated solely from thermally grown silica, based on an air-clad rib waveguide racetrack resonator suspended on a silica membrane. A Q-factor of 3×10^3 was achieved in a strongly overcoupled configuration. Here we present a similar concept based on a suspended ring resonator fabricated from thermally grown silica. We demonstrate that an improvement by more than three orders of magnitude to a Q-factor of 3.7×10^6 was possible by optimizing optical design and process technology w.r.t. phase-matching and coupling regime in a micro-ring resonator.

II. Methods

A. Design

Two main design goals need to be addressed: First, phase-matching between ring-resonator and coupler waveguide must be achieved to ensure efficient coupling to the resonator. Second, the cross coupling coefficient k must be set so that operation in the desired coupling regime, usually critical coupling, is achieved.

We employ a rib waveguide design for both the resonator and the coupling waveguide geometry. Since the devices are to be fabricated from thermally grown silica on silicon without any additional materials, a thin silica membrane is necessary to support the air-clad wave-guiding structures. The geometry parameters are shown in Fig. 1: Waveguide width w, oxide thickness h, membrane height m, coupling gap d, and ring radius R. Coupling between resonator modes and waveguide coupler modes as well as loss per round-trip is described by the single-pass amplitude transmission coefficient a, the self-coupling coefficient r, and the cross-coupling coefficient k, as described by Bogaerts *et al.* [14].

A symmetric directional coupler layout as shown in Fig. 1 is chosen over straight, concentric and weakly tapered layouts [15] to ensure optimal phase matching. We use a numeric mode solver (Fimmwave, Photon Design) to find the fundamental modes of the resonator and waveguide coupler, and determine the amplitude cross coupling coefficient k between the fundamental modes for a given geometry. To achieve critical coupling the power coupled to the ring resonator must be equal to the power loss per round-trip under the assumption that there are no losses in the coupling section ($1 - a^2 = k^2 \Rightarrow a = r$), so that k decreases with decreasing round trip loss. The corresponding loaded Q-factors are determined as described in [14]. Since the loss is unknown we need to design geometries for a range of different k.

Our design is optimized for operation at 1064 nm, and the ring radius R is set to 0.5 mm, which results in a free spectral range for the ring resonator of 60 GHz. Rib geometry parameters are set to oxide thickness $h = 2$ μm, rib waveguide width $w = 1.4$ μm. To reduce loss at the coupling section a membrane thickness of $m = 0.8$ μm ensures single-mode wave-guiding for waveguide dimensions larger than the wavelength. Fig. 2 shows the dependence of the numerically determined amplitude cross coupling coefficient k on the coupling gap d. The coupling gap d is varied from 0.5 μm to 1.8 μm, and the corresponding loaded Q-factors at k in case of critical coupling are indicated with a dashed line, as described above. The amplitude cross coupling coefficient k is larger for TE-modes than for TM-modes, in contrast to common SOI-devices [14] due to their geometrical differences.

To allow for efficient coupling of laser light to the resonator chip the waveguide width w is tapered up to 2 μm at the chip facets. Furthermore, the waveguide is angled at the facet to suppress unwanted Fabry-Pérot-modes.

B. Fabrication

A schematic overview of the fabricated structure is given in Fig. 3. The devices were fabricated on commercially available 3" Si substrate wafers (Simat) coated with 2 μm thermally grown silica. Photolithography and fluoride-based reactive ion etching (RIE) steps are used to fabricate rib waveguide,

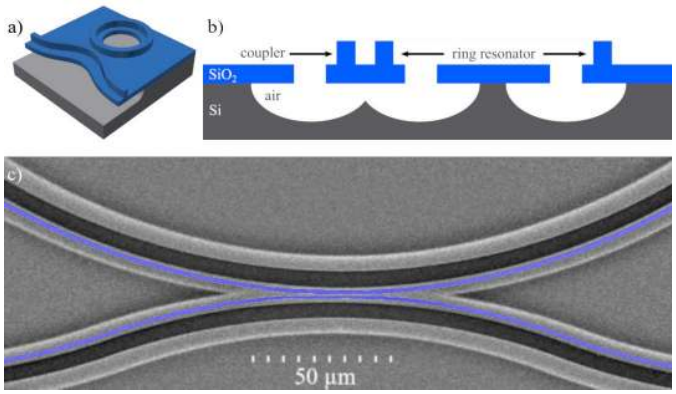

Fig. 3. a) Schematic overview of the processed structure. b) Cross-section of the coupling area. Resonator and waveguide coupler are underetched, the whole structure is supported by the thin membrane. Etch trenches are located on the inside of the ring resonator and on one side of the waveguide coupler. c) Scanning electron micrograph of the coupling area (Top-view) The location of the waveguides is highlighted in blue.

facets, etch trenches, and ring resonator structures. After that, an isotropic wet-etch with a $HNO_3/HF/C_2H_4O_2$ mixture is used to selectively remove the Si beneath the wave-guiding areas. The etch trenches span the whole chip length to release the stress in the oxide layer, thereby preventing the stress-induced deformations [13] described by Chen *et al.* from occurring. Then a thick resist layer is applied for mechanical protection and individual chips are diced with a wafer saw. The fabrication process will be presented elsewhere [16].

C. Characterization

We use a temperature stabilized distributed feedback laser with an emission wavelength of 1064 nm for transmission spectroscopy measurements. The laser frequency is scanned over a spectral range of 140 GHz by applying a triangular modulation signal (0.25 Hz) to the laser current. Calibration of the laser-scan is done with an optical wavemeter (WS/7 MC8, High Finesse) with an absolute accuracy of 60 MHz. A lensed fiber with a spot size of 2 μm (OZ Optics) is used to couple light to the resonator chip. The lensed fiber is positioned by piezo actuators with a minimal step size of 1 nm and a closed loop sensor resolution of 1 nm (Smaract). We employ a half-wave-plate to set the input polarization. To account for the variation of laser power during a laser scan we use a fiber splitter to generate a power reference signal with a photo detector.

The transmitted light is collimated with an aspheric lens (C392TME-C, Thorlabs) and measured with a photodetector (PDA100A, Thorlabs). All signals are simultaneously sampled with an AD-converter (PCIe-6363, National Instruments) at 100 kHz sampling rate. The transmission spectrum is normalized to the power reference signal detected at the power monitor, and the resulting quantity is scaled such that the transmitted signal equals 1 far off resonance.

III. Results and Discussion

Fig. 4a) shows a typical transmission spectrum measurement for a device with geometry parameters as described above, with a coupling gap of 1.2 μm for TE (blue) and TM (red) polarization. We measure a free spectral range of 60.9 GHz for both polarizations, which matches the design prediction.

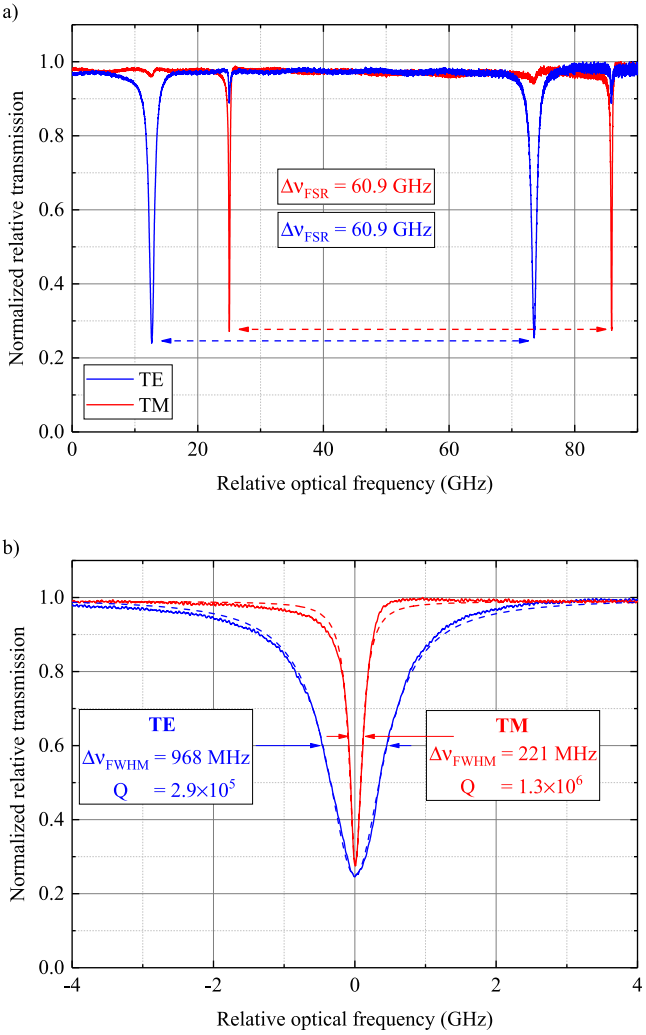

Fig. 4. a) Normalized relative transmission spectrum for the designed device geometry with a coupling gap of d of 1.2 μm at TE (blue) and TM (red) polarization measured at 1064 nm. The free spectral range of 60.9 GHz corresponds to the ring diameter of 1 mm. Higher order modes are not excited. b) Lorentzian fits of TE and TM resonance dips delivers a Q-factor difference of nearly one order of magnitude.

Fig. 4b) shows that both resonances are close to critical coupling. Higher order resonator modes are not excited. A fit of the Lorentzian-shaped transmission dip delivers a Q-factor of $2.9 \times 10^5 (\Delta\nu_{\mathrm{FWHM}} = 968$ MHz) for the TE-mode and a Q-factor of 1.3×10^5 ($\Delta\nu_{\mathrm{FWHM}} = 221$ MHz) for the TM-mode. TM modes are expected to deliver higher Q-factors than TE modes because scattering loss at the rib surface is smaller for TM modes due to stronger lateral confinement. The difference between simulated and measured Q-factors close to critical coupling is attributed to additional loss at the coupler, which is not included in the theoretical model. Additionally, the model assumes perfect critical coupling, which we do not achieve. The degrading signal to noise ratio towards higher relative optical frequency is a result of the decreasing laser power at higher optical frequencies.

To be able to assess the quality of the fabricated resonators independent of the coupling area we measure a weakly coupled resonator mode in another device with a different coupling geometry that ensures operation in the under-coupled regime ($w = 1.6$ μm, $h = 2.0$ μm, $m = 0.5$ μm, $d = 1.0$ μm).

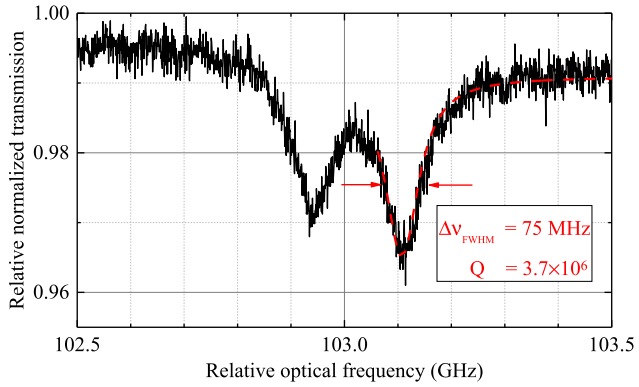

Fig. 5. Resonance spectrum of a weakly coupled resonator used to determine an upper bound for the waveguide loss of 2.0 dB/m. Mode-splitting occurs due to coupling of clockwise and counterclockwise propagating fundamental modes.

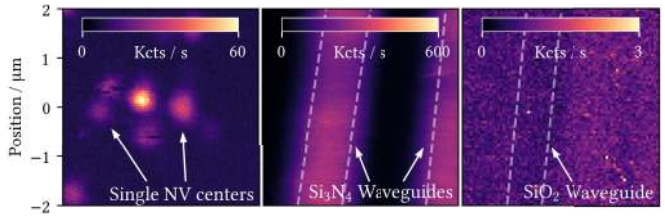

Fig. 6. Comparison of the confocally detected fluorescence signal for different samples. On the left the fluorescence signal of single nitrogen-vacancy centers in diamond is shown for reference at 30 kcts/s. The Si_3N_4 waveguides in the center show ten times as much fluorescence which makes them unsuitable for single-photon experiments. The silica devices presented in this article show fluorescence well below that of the single quantum emitters, highlighting the usability of the devices for single-photon experiments.

The result is shown in Fig. 5, the intrinsic Q-factor is determined to be 3.7×10^6. From this an upper bound for the waveguide propagation loss is calculated to be 2.0 dB/m [17]. As the Q-factor is larger by a factor of three in comparison to the almost critically coupled device, mode-splitting due to coupling of clockwise and counter-clockwise propagating WGMs is observed.

Fig. 6) compares confocal fluorescence scans of a typical Si_3N_4 on SiO_2 waveguide chip, and a silica device as presented in this article to a reference scan of single quantum emitters (nitrogen-vacancy color centers in diamond) on a glass substrate, as used in single photon experiments [18]. The Si_3N_4 on SiO_2 waveguide chip is not suitable for single quantum emitter experiments as it's fluorescence background is ten times higher than that of the emitters themselves. On the contrary, the silica devices presented in this article show a barely detectable fluorescence background of only 2 kcts/s, exemplifying the unique attributes of devices fabricated solely from thermally grown silica. Experimental conditions were kept constant for the three confocal scans (excitation wavelength $\lambda_{ex} = 532$ nm, excitation power $P_{ex} = 0.5$ mW and detection window from 620 nm to 800 nm).

IV. Conclusion

We have demonstrated the design and fabrication of a micro-ring resonator chip with integrated rib waveguide for evanescent coupling. It is solely based on silica thermally grown on Si, and hence avoids drawbacks such as excess fluorescence or material absorption in the UV wavelength range that are related to devices solely or partially incorporating other materials. The devices presented here deliver an intrinsic Q-factor of 3.7×10^6, exceeding the Q-factors of similar devices presented by [13] by three orders of magnitude. To our knowledge this is the highest Q-factor achieved in an integrated system made solely of thermally grown silica. This advancement was made possible by a ring resonator design based on a thicker oxide layer, the introduction of stress-relieving etch trenches as well as an optimized coupling gap design to achieve operation close to the critical coupling regime. We expect that it is possible to increase the intrinsic Q-factor by at least one order of magnitude through further optimization of the design and process technology.

References

[1] Y. Lin *et al.*, "Characterization of hybrid InP-TriPleX photonic integrated tunable lasers based on silicon nitride (Si_3N_4/SiO_2) microring resonators for optical coherent system," *IEEE Photon. J.*, vol. 10, no. 3, pp. 1–8, Jun. 2018.

[2] R. Luo, H. Jiang, S. Rogers, H. Liang, Y. He, and Q. Lin, "On-chip second-harmonic generation and broadband parametric down-conversion in a lithium niobate microresonator," *Opt. Express*, vol. 25, no. 20, pp. 24531–24539, Oct. 2017.

[3] P. Del'Haye, T. Herr, E. Gavartin, M. L. Gorodetsky, R. Holzwarth, and T. J. Kippenberg, "Octave spanning tunable frequency comb from a microresonator," *Phys. Rev. Lett.*, vol. 107, no. 6, 2011, Art. no. 063901.

[4] J. Lim, A. A. Savchenkov, A. B. Matsko, S.-W. Huang, L. Maleki, and C. W. Wong, "Microresonator-stabilized extended-cavity diode laser for supercavity frequency stabilization," *Opt. Lett.*, vol. 42, no. 7, p. 1249, Apr. 2017.

[5] T. J. Kippenberg *et al.*, "Fabrication and coupling to planar high-Q silica disk microcavities," *Appl. Phys. Lett.*, vol. 83, no. 4, pp. 797–799, 2003.

[6] P. Trocha *et al.*, "Ultrafast optical ranging using microresonator soliton frequency combs," *Science*, vol. 359, no. 6378, pp. 887–891, Feb. 2018.

[7] A. Naiman, B. Desiatov, L. Stern, N. Mazurski, J. Shappir, and U. Levy, "Ultrahigh-Q silicon resonators in a planarized local oxidation of silicon platform," *Opt. Lett.*, vol. 40, no. 9, pp. 1892–1895, 2015.

[8] X. Ji *et al.*, "Ultra-low-loss on-chip resonators with sub-milliwatt parametric oscillation threshold," *Optica*, vol. 4, no. 6, pp. 619–624, 2017.

[9] B. J. M. Hausmann, I. Bulu, V. Venkataraman, P. Deotare, and M. Loncar, "Diamond nonlinear photonics," *Nature Photon.*, vol. 8, no. 5, pp. 369–374, 2014.

[10] H. Lee *et al.*, "Chemically etched ultrahigh-Q wedge-resonator on a silicon chip," *Nature Photon.*, vol. 6, no. 6, pp. 369–373, 2012.

[11] M. Ferrera *et al.*, "Low-power continuous-wave nonlinear optics in doped silica glass integrated waveguide structures," *Nature Photon.*, vol. 2, no. 12, pp. 737–740, 2008.

[12] S. H. Lee *et al.*, "Towards visible soliton microcomb generation," *Nature Commun.*, vol. 8, no. 1, 2017, Art. no.1295.

[13] P. Chen, Y. Zhu, Y. Shi, D. Dai, and S. He, "Fabrication and characterization of suspended SiO_2 ridge optical waveguides and the devices," *Opt. Express*, vol. 20, no. 20, pp. 22531–22536, Sep. 2012.

[14] W. Bogaerts *et al.*, "Silicon microring resonators," *Laser, Photon. Rev.*, vol. 6, no. 1, pp. 47–73, 2012.

[15] D. T. Spencer, J. F. Bauters, M. J. R. Heck, and J. E. Bowers, "Integrated waveguide coupled Si_3N_4 resonators in the ultrahigh-Q regime," *Optica*, vol. 1, no. 3, pp. 153–157, 2014.

[16] A. Thies *et al.*, "Process technology and design for the fabrication of passive optical devices based on silicon oxide," unpublished.

[17] P. Rabiei, W. H. Steier, C. Zhang, and L. R. Dalton, "Polymer micro-ring filters and modulators," *J. Lightw. Technol.*, vol. 20, no. 11, pp. 1968–1975, Nov. 2002.

[18] Q. Shi *et al.*, "Wiring up pre-characterized single-photon emitters by laser lithography," *Sci. Rep.*, vol. 6, Aug. 2016, Art. no. 31135.